

A DETECTION SYSTEM FOR ENERGETIC LIGHT HEAVY IONS

C.P.M. VAN ENGELEN, R. JELMERSMA, A. VAN DEN BRINK and R. KAMERMANS

Fysisch Laboratorium, Rijksuniversiteit Utrecht, PO Box 80.000, 3508 TA Utrecht, The Netherlands

Received 18 April 1984 and in revised form 4 July 1984

A light heavy ion detection system which consists of a gas-filled ionization chamber (IC) connected to a scattering chamber via a time-of-flight (TOF) system has been constructed. The entrance window of the IC has an area of $14 \times 40 \text{ cm}^2$, the active depth is 115 cm. Filled with CF_4 at a pressure of 350 Torr, the energy range for ^{12}C and ^{40}Ar is 5–20 MeV/ A and 6–30 MeV/ A , respectively. The TOF system consists of two parallel plate avalanche counters with a flightpath of 70 cm or 170 cm in between. The IC has been tested with ^{12}C ions at an energy of 39 MeV. The energy resolution of the IC (1.1%) is mainly determined by the energy straggling in the foils of the TOF system and the ionization chamber. The energy-loss resolution is 3.5%, the horizontal position resolution varies between 6 and 20 mm and the vertical position resolution is 2 mm. The time resolution of the TOF system ranges from 800 ps for ^4He at 5.0 MeV, to 280 ps for ^{28}Si at 55 MeV.

1. Introduction

In peripheral collisions between medium heavy targets ($A = 40\text{--}60$) and light heavy ions ($A = 16\text{--}40$) at intermediate energies ($E = 10\text{--}30 \text{ MeV}/A$) a large part of the cross section has a projectile-like fragment and one or more light ($Z \leq 2$) particles in the final state [1,2]. In order to detect the highly energetic projectile-like fragments, a system was constructed which consists of two major parts: (1) a scattering chamber with a diameter of 60 cm in which several light-particle telescopes can be placed and (2) a light heavy ion detection system which consists of a gas-filled ionization chamber (IC) placed at 1 m distance from the target with a time-of-flight (TOF) system in between (see fig. 1).

The use of a gas-filled ionization chamber [3–8] has several advantages in comparison to surface barrier detectors: (1) it can have a large solid angle (50 msr), (2) it does not suffer from radiation damage, (3) by adjusting the pressure in the detector the effective thickness can be changed easily and (4) it does not show a pulse-height defect due to nuclear collisions or plasma recombination. Also, simple techniques are known to measure the position of the ions in the detector.

Two gas-filled timing detectors (parallel plate avalanche counters, PPAC [3,6,9]) are the main components of the TOF system. This system is positioned in the flight path of the ions from the target to the ionization chamber.

The ionization chamber and the TOF system were tested with ^{12}C ($E = 39 \text{ MeV}$) beams accelerated by the EN tandem in Utrecht. Energy, position and time resolutions, obtained from the data, have been compared

with calculated values. As a result of the test runs small improvements in the setup have been carried through.

Sections 2 and 3 will give an outline of the construction and characteristics of the IC and the PPACs, respectively. Data on the performance of the IC and the PPACs will be presented and discussed in sections 4 and 5, respectively. The last section (6) will give some concluding remarks.

2. The ionization chamber

The ionization chamber (fig. 2) is a slightly modified version of the “Mammut” detector developed at GSI Darmstadt [5]. It is connected to the scattering chamber via a flight path with a length of 0.7 m or 1.7 m (see also fig. 1, shown is the 0.7 m flight path). Together with the scattering chamber it can be rotated over 60° , covering all angles between 0° and 70° . The large entrance window (area $14 \times 40 \text{ cm}^2$, $d\Omega = 50 \text{ msr}$ with a flight path of 0.7 m) consists of a perspex frame which enters the detector for 7 cm. A thin ($2 \mu\text{m}$) mylar foil, supported by horizontally stretched steel wires (diameter 0.1 mm) with a spacing of 2.5 mm, is glued to the perspex frame. Five vertical supports (1.5 mm thick) are positioned every 70 mm. This geometry yields a transmission of 94%. The window can stand a pressure difference of about 350 Torr. The support wires are connected to a potential divider in order to achieve a homogeneous electrical field along the foil. Field shaping electrodes in the middle and on the top and bottom sides of the perspex frame are also connected to the potential divider.

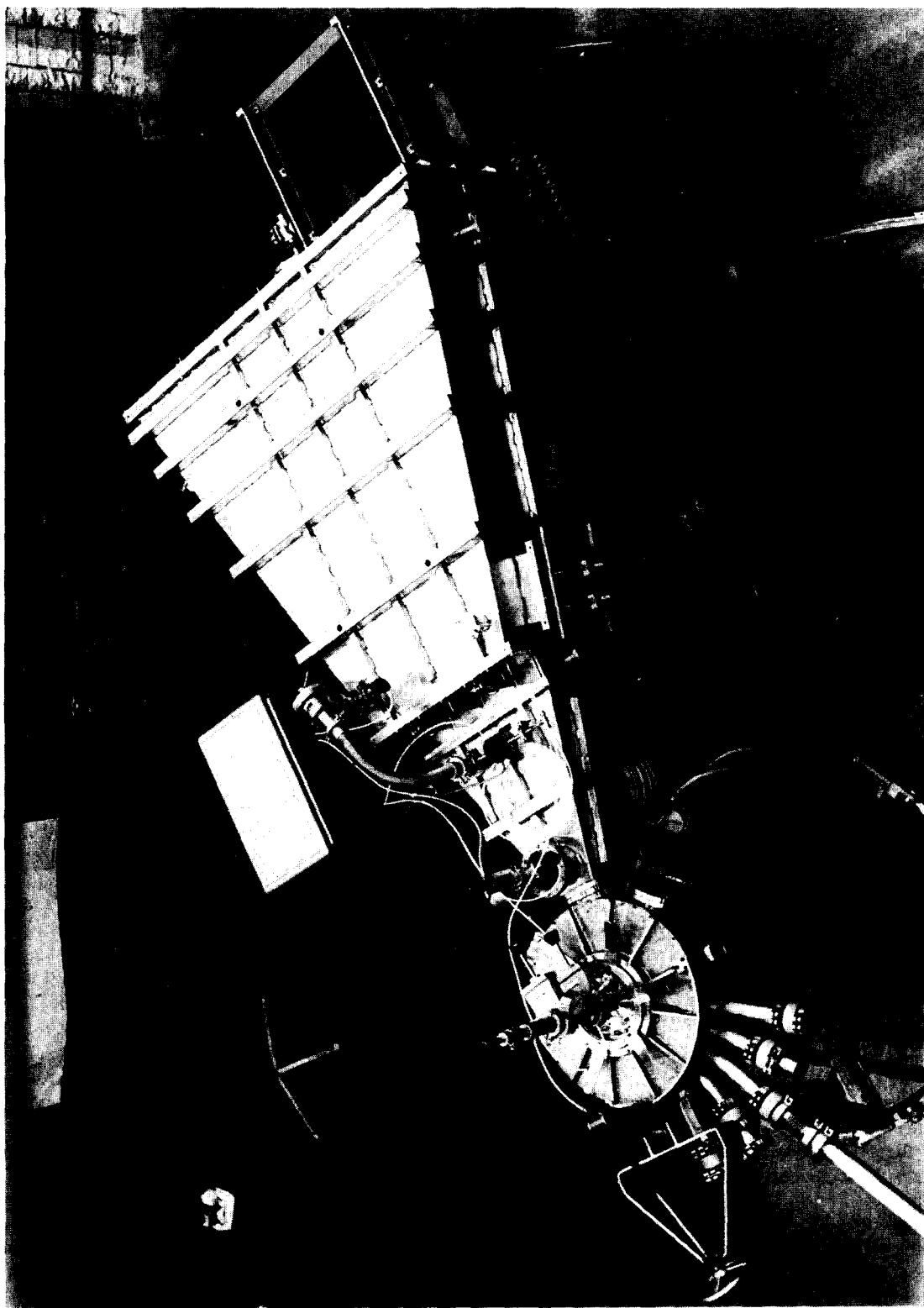


Fig. 1. Picture of the experimental setup.

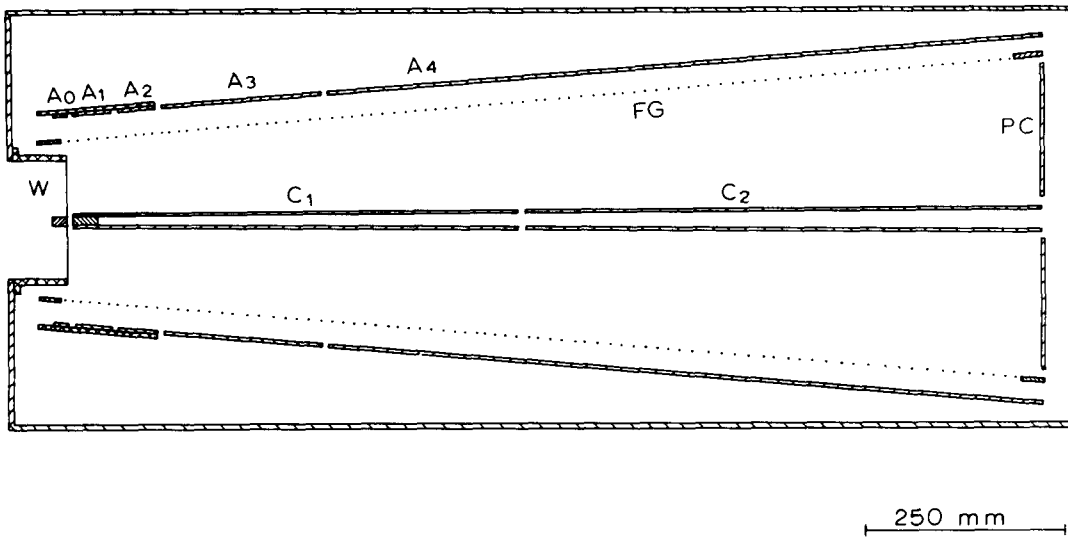


Fig. 2. Schematic side view of the heavy-ion ionization chamber. W: mylar window ($2\ \mu\text{m}$), C_1 and C_2 : cathodes, negative bias ($0.5\text{--}2.5\ \text{kV}$), FG: Frisch grids, $50\ \mu\text{m}$ Cu-Be wires spaced $1\ \text{mm}$ apart, grounded, $A_0\text{--}A_4$: anodes, positive bias ($0.5\text{--}1\ \text{kV}$), A_1 and A_2 are position sensitive, and PC: printed circuit board with stripes which form a potential divider. The lower part of the ionization chamber is identical to the upper part.

Four cathodes, positioned in the middle of the chamber divide it into two symmetrical parts. The upper and lower cathode in the front part of the detector are electrically coupled together as well as the two cathodes in the back part of the detector. All cathodes are put on a negative bias with respect to the grounded Frisch grid. Between the cathode and the Frisch grid potential dividers, made out of stripes etched on printed circuit board, are used to shield the sensitive volume of the counter from field disturbances induced by the grounded walls of the detector chamber. The Frisch grid consists of a frame made out of $2\ \text{mm}$ thick steel on which 1200 Cu-Be wires (diameter $50\ \mu\text{m}$) are glued with a spacing of $1\ \text{mm}$. The distance between grid and cathode varies between $10\ \text{cm}$ and $15\ \text{cm}$. This inclination allows the particles to enter the detector with a large out-of-plane angle (vertical position) without hitting the grid.

A drawing of the anode layout is given in fig. 3. The first three anodes (A_0 , A_1 and A_2) are made out of printed circuit board and are fixed on a $2\ \text{mm}$ thick perspex plate. The anode A_0 is positioned for the major part above the perspex frame of the entrance window and is mainly used for field shaping purposes. It is electrically connected to anode A_3 . Both anodes A_1 and A_2 have been made position sensitive in the horizontal direction by using the "saw-tooth" method [10] (see fig. 4). The anodes A_3 and A_4 are made out of $2\ \text{mm}$ thick stainless steel plates. The Frisch grid and anodes are positioned parallel to each other at a distance of $3\ \text{cm}$. All anodes operate at the same positive bias. To prevent electrons from hitting the grid wires the electrical field between anodes and grid is chosen twice as high as the

field between cathode and grid [8]. A minimum condition for the electrical field is also given by the risetime of the anode signals which should be less than $0.5\ \mu\text{s}$.

The vertical position (y) is determined from the drift time of the electrons from the particle track to the Frisch grid. A start signal is obtained from one of the timing detectors in front of the ionization chamber (see

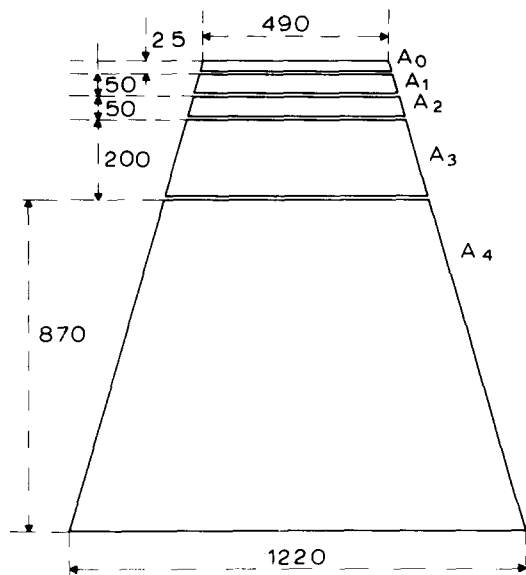


Fig. 3. Dimensions of the five anodes $A_0\text{--}A_4$ in mm. The anodes A_1 and A_2 are position sensitive in the horizontal (x) direction.

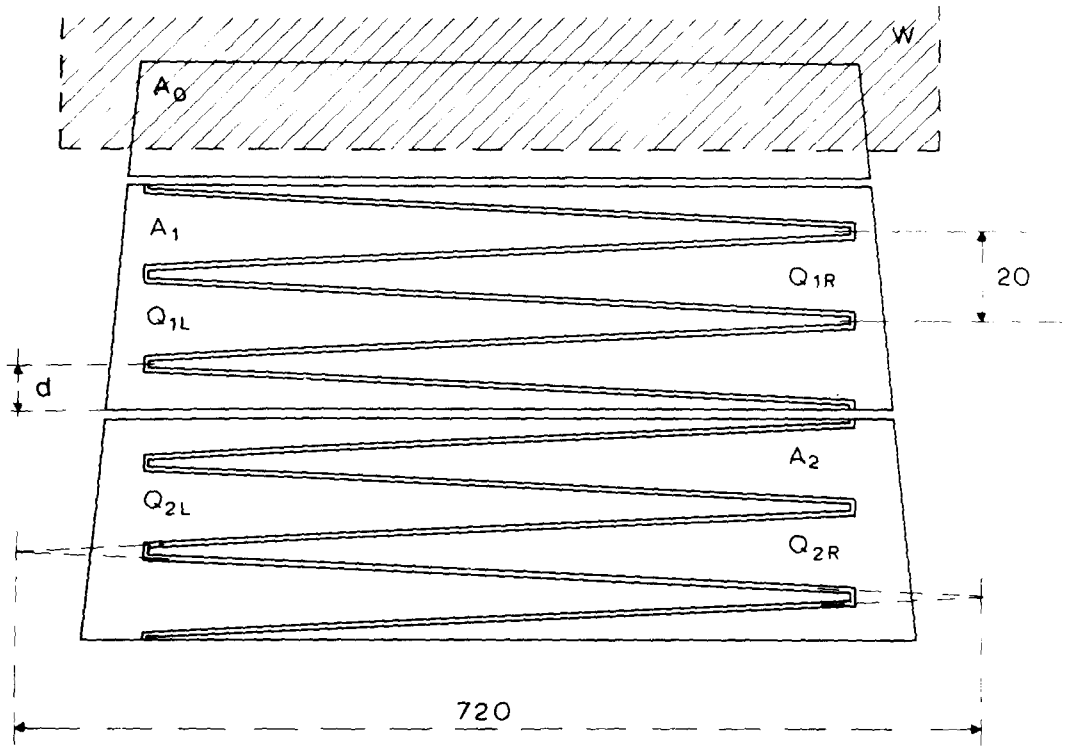


Fig. 4. Detailed view of the first three anodes A_0 – A_2 (dimensions in mm). W gives the projection of the entrance window on anode A_0 . Q_{1L} , Q_{1R} , Q_{2L} and Q_{2R} denote the signals from the anodes, anode A_0 is electrically connected to A_3 , d is the width of one segment (10 mm).

section 3). The stop signal is obtained from the signal of the second or third anode.

The horizontal position (x) is measured by dividing the first and second anode into two parts, which are electrically separated. Each anode consists out of 5 segments with a width d (fig. 4). If the stopping power is constant over one segment of the anode, the horizontal position x of the particle ($-1 \leq x \leq 1$) will be given by [10]:

$$x = \frac{E_R - E_L}{E_R + E_L}, \quad (1)$$

where E_R and E_L are the energy losses under the right and left part of the anode.

The signals of 14 charge-sensitive preamplifiers (12 anode signals and 2 cathode signals) are processed by home-built main amplifiers which are connected to 2K CAMAC ADCs. The signal from anode A_2 or A_3 is also fed into a timing single channel analyzer (Ortec 455) in order to obtain a stop signal needed for the y readout.

The large volume of the IC can be pumped down to a pressure of 0.1 Torr with a roughing pump. By opening a large valve between the flight path and the IC, a pressure of 10^{-4} Torr can be reached in the ionization

chamber before filling the chamber with the detector gas. A differential pressure meter [11] measures the pressure difference between the IC and the flight path with an accuracy of 0.5 Torr. Since the radiation damage to the gas is small no flow system has been installed.

Isobutane (C_4H_{10}) and carbon tetrafluoride (CF_4) are used as gas fillings since these gasses yield a maximum stopping power. The pressure in the IC is limited by the entrance foil to 350 Torr. With CF_4 at this pressure the maximum energy for which incoming particles are fully stopped in the sensitive depth of the chamber (115 cm) is 20 MeV/A for ^{12}C ions and 30 MeV/A for ^{40}Ar ions. The minimum particle energy is determined by the condition that at most 75% of the particle energy is lost under the first anode A_1 (5 cm deep). Additionally the energy loss under the first anode A_1 should be larger than 15 MeV to achieve a sufficient position resolution in the horizontal plane (see section 4). With CF_4 at a pressure of 350 Torr the minimum energy is 5 MeV/A for ^{12}C and 6 MeV/A for ^{40}Ar . Stopping powers have been calculated with formulas taken from ref. [12]. Corrections have been made for energy losses in the entrance foil.

3. The time-of-flight system

There are two reasons to install a time-of-flight (TOF) system in front of the heavy-ion detector. First of all the mass of the incident particle can be determined from its velocity as measured by the TOF system and its energy, measured by the ionization chamber. Secondly, since all signals from the ionization chamber are delayed by a few microseconds, due to the electron drift time in gasses, no prompt signal in the nanosecond region is available from the ionization chamber which can be used for coincidence studies. Timing detectors with a large area can be divided into two types, (1) the low pressure multiwire proportional chamber (LPMWPC [13]) and (2) the parallel plate avalanche counter (PPAC [3,6,9]). In this setup two PPACs have been installed because of the simplicity of the detector design.

The small start detector of the TOF system is positioned in the scattering chamber at a distance of 20 cm from the target. Its active area is $50 \times 100 \text{ mm}^2$ and covers the complete solid angle of the ionization chamber. The large stop detector with a total active area of $140 \times 390 \text{ mm}^2$ is placed just in front of the ionization chamber. The pressure foils are made out of $2 \mu\text{m}$ thick non-aluminized mylar whereas the electrodes are made of $2 \mu\text{m}$ thick stretched, aluminized mylar foils, which are glued onto epoxy glass frames. To ensure good electrical connections to the electrode foils a contact ring is fixed directly on the aluminized side of the foil with a 2 mm screw. Small plastic rings with a thickness of 2 mm are used to keep the spacing between the anode and the cathode foil at 2 mm within 10 μm .

An estimate of the electronic time resolution δt_e of the PPAC is given by [3]:

$$\delta t_e = t_r V_n / V_p, \quad (2)$$

where t_r is the risetime of the signal, V_p is the pulse height and V_n is the noise on the signal. Eq. (2) shows that in order to minimise the time resolution the components of the PPAC should be chosen in such a way as to minimise t_r and to maximise V_p . The electronic risetime of the system is given by:

$$t_{re} = RC_{ppac}, \quad (3)$$

where R is the input resistance of the preamplifier (50 Ω) and C_{ppac} is the capacitance between the PPAC anode and cathode. To achieve a minimum risetime, t_{re} should be equal to or less than the intrinsic risetime t_0 of the PPAC pulse. The small PPAC has $C_{ppac} = 70 \text{ pF}$, which gives $t_{re} = 3.5 \text{ ns}$. Since this value is of the order of the intrinsic risetime t_0 (1–2 ns) no large improvement of δt_e can be obtained by reducing C_{ppac} . For the large PPAC however, the value of C_{ppac} for the total active area is 400 pF. This would yield a risetime of 20 ns. During the test runs the large PPAC was therefore

divided into two electrically divided parts (with $C_{ppac} \approx 200 \text{ pF}$), with separate preamplifiers connected to both parts.

The pressure and gas flow in the PPACs is maintained by an electronic circuit which consists of a differential pressure meter between the PPACs and the flightpath (accuracy 0.05 Torr), a pressure readout unit, a pressure control unit and a regulation valve. The system is pumped by a separate roughing pump. A needle valve with flow meter is used to adjust the amount of gas flow (typically 10^{20} molecules/s). This totally refreshes the gas in the PPACs every 15 min. The pressure control unit keeps the pressure constant within 0.02 Torr.

4. The performance of the ionization chamber

First tests with the ionization chamber were performed with a ^{12}C beam ($E = 39 \text{ MeV}$), accelerated by the EN tandem of the R.J. Van de Graaff Laboratory in Utrecht. The centre of the detector was positioned at an angle of 30° with respect to the beam. A thin gold target ($320 \mu\text{g}/\text{cm}^2$) was used to scatter beam particles into the detector. To measure the position resolution and the position dependence of the energy signals a perspex mask with 80 holes (each with a diameter of 1 mm) was placed just in front of the detector. The holes were divided in 8 rows of 10 holes with a vertical spacing of 10 mm and a horizontal spacing of 35 mm. Test runs were performed with and without a PPAC placed in front of the IC in order to study the influence of energy straggling in the foils of the PPAC on the energy signals of the IC. Since the IC is fully symmetric only results for the upper part of the chamber will be given.

Two kinds of gases were used, both at two pressures: isobutane (C_4H_{10}) at pressures of 38 Torr and 150 Torr and carbon tetrafluoride (CF_4) at pressures of 40 Torr and 160 Torr. Other gases were not considered, since the large stopping power of C_4H_{10} and CF_4 is needed to stop very energetic (10–30 MeV/A) particles. The ranges of ^{12}C , calculated with the stopping powers taken from ref. [12], were 12 cm and 50 cm for the high and low pressures, respectively. At the higher pressures, the incoming particles were almost completely stopped under the second anode. Therefore, only anode 1 was used as a position sensitive device. The left and right side of anode 2 were electrically connected with each other and the signal was used as a stop signal for the γ readout.

In order to obtain a drift time between 5 and 10 μs the cathode bias was adjusted at 500 and 1500 V for C_4H_{10} and at 70 and 200 V for CF_4 , at low and high pressure, respectively. Due to the non-rectangular geometry the electrical field at the end of the detector is a factor 1.5 lower than at the front of the detector. This gives a maximum variation in electron drift time of a

factor 2–3 for anode A₄. During the test experiments however, the range of the incoming ions was limited to 50 cm, which gives a variation in drift time of a factor 1.3 for anode A₄. This did not influence the energy signals. The different values of the electrical field for C₄H₁₀ and CF₄ at almost the same pressures show that the mean free path of electrons in CF₄ is much larger than in C₄H₁₀ (ref. [14], eqs. (1,9)).

Data were collected in event by event mode with the computer code SPECTR [15], running on a PDP 11/34 computer. The off-line analysis has been performed on a PDP 11/70 computer with the same code.

4.1. The total-energy signals

In the off-line analysis of the data, the digitized signals of the anodes have been summed in order to obtain the total energy dissipated in the IC. The ADC words have been calibrated by the use of pulser data. During the experiment, the pulser was connected to all preamplifiers via the test inputs of the preamplifiers to observe possible gain shifts.

Separate energy spectra have been collected for particles which entered the detector through each of the 40 holes of the upper part of the mask by using software gates in the *x* and *y* coordinates. The positions of the full energy peaks were corrected for differences in energy resulting from kinematics and energy losses in the foils.

For C₄H₁₀ at a pressure of 150 Torr, a systematic dependence of the energy signals on the *y* coordinate exists: the energy signals are smaller for longer electron drift paths. This variation amounts from 0.8% to 1.2% per centimeter drift path. For C₄H₁₀ at a pressure of 38 Torr, the effect is reduced to less than 0.2% per centimeter. CF₄ does not show this dependence. The effect seen with C₄H₁₀ at 150 Torr is probably due to recombination of electrons [8]. Applying a higher bias on the

cathode which is not feasible yet, would give a smaller drift time and probably reduce this effect. Capture of electrons by electronegative gasses [8,16] can be excluded since with CF₄ no systematic dependence of the energy signals has been observed.

The calibration factor from channels to keV has been found by calculating the energy losses of the ¹²C particles in the target, the foils and a 5 mm dead layer of gas in the IC (stopping powers have been taken from ref. [12]). The error in the energy-loss calculation is 25%. This leads to an error in the calibration factor of 1.6% for the data without PPAC and 6% for the data with PPAC. For the two gases, the calibration factors agree with each other within 5%. For CF₄, the calibration factor is a factor 1.25 larger than for C₄H₁₀. Since the mean energy to create an electron-ion pair in C₄H₁₀ is 23 eV (*W_i*, table 1 in ref. [16]), this energy is 29 eV for CF₄. This value is comparable to the value of *W_i* given for CH₄ [16]: *W_i* = 28 eV.

The mean values of the total-energy resolution (δE) are given in table 1 for the eight experimental situations (C₄H₁₀ and CF₄, low and high pressure, with and without PPAC). The total-energy resolution has three major contributions: (1) energy-loss straggling in the target, the foils and the dead layer of gas in the IC, (2) the inhomogeneity of the target and the PPAC foils and (3) the preamplifier noise. The first contribution can be divided in the classical Bohr straggling (δE_B) and, since the detector is tested with light-heavy ions, a term due to fluctuations in the effective charge of the ion (δE_{cf}) [17]:

$$\delta E_B = 0.928 Q_i (\Delta x Z_a / M_a)^{1/2}, \quad (4)$$

and

$$\delta E_{cf} = K (Z_i)^{1/2} (\Delta E)^{0.53}, \quad (5)$$

with *Q_i* the mean effective charge of the ion, *Z_a* the number of electrons per molecule of the absorber, *M_a* the molecular weight in grams of the absorber mole-

Table 1

The energy resolution of the IC as a function of the counting gas and the gas pressure (*P*). PPAC: 1 indicates a PPAC in front of the IC, δE : measured total-energy resolution (fwhm), δE_{str} : calculated straggling contribution, δE_{inh} : calculated inhomogeneity contribution, δE_n : noise contribution, δE_{tot} : calculated total-energy resolution (see text).

Gas	<i>P</i> (Torr)	PPAC	δE (keV)	δE_{str} (keV)	δE_{inh} (keV)	δE_n (keV)	δE_{tot} (keV)
C ₄ H ₁₀	38	0	260	160	60	170	240
CF ₄	40	0	310	160	60	230	290
C ₄ H ₁₀	150	0	300	190	60	120	230
CF ₄	160	0	260	200	60	150	260
C ₄ H ₁₀	38	1	370	330	120	170	390
CF ₄	40	1	400	330	120	230	420
C ₄ H ₁₀	150	1	410	360	120	120	400
CF ₄	160	1	360	360	120	150	410

cules, Δx the absorber thickness in g/cm², K the absorber material constant, Z_i the nuclear charge of the incident ion and ΔE the energy loss in the absorber in MeV. The total fwhm due to energy loss straggling (δE_{str}) is given by:

$$\delta E_{\text{str}} = (\delta E_B^2 + \delta E_{\text{cf}}^2) \frac{S(E - \Delta E)}{S(E)}, \quad (6)$$

where $S(E)$ is the stopping power in the absorber. The last term is a correction for finite energy losses in the absorber [17]. The average charge stage Q_i of the incident ion is calculated according to formulas given in ref. [12]. The factor K has been measured for C1 ions in isobutane [18]: $K = 0.035 \text{ MeV}^{0.47}$, and for ³²S and ⁵⁸Ni ions in polypropylene [7]: $K = 0.037 \text{ MeV}^{0.47}$. Since these values differ very little, the value of K for ¹²C ions in mylar, C₄H₁₀ and CF₄ has been taken as $K = 0.035 \text{ MeV}^{0.47}$. Calculated values of δE_{str} are given in table 1.

Since the mask limited the size of the irradiated IC foil to 0.8 mm² per hole, no contribution due to the inhomogeneity of the IC foil has been taken into account. Inhomogeneity of the PPAC foils and of the target have been taken into account by assuming a 5% thickness variation of the foils. The spread in effective target thickness due to the scattering angle of 30°, introduces an additional 15% variation of the energy loss in the target. Values of the total inhomogeneity contribution (δE_{inh}) are given in table 1.

The noise contribution to the energy resolution has been measured with pulser data. Anode A₄ only contributed to the total signal at the pressures of 38 and 40 Torr. Since the capacitance of anode A₄ is relatively large (500 pF), its noise contribution is also large. Therefore the noise contribution for the low-pressure data is twice as high as the noise contribution for the high-pressure data. The noise contribution in channels is the same for C₄H₁₀ and CF₄. Since the calibration factors from channels to keV differ by a factor of 1.25,

the noise contribution for CF₄ is a factor 1.25 larger than the noise contribution for C₄H₁₀.

The quadratic sum of δE_{str} , δE_{inh} and δE_n (δE_{tot}) is given in table 1. For the data without the PPAC the agreement between measured and calculated values is reasonable, except for C₄H₁₀ at 150 Torr. This discrepancy might be connected to the recombination of electrons as observed with C₄H₁₀ at this pressure. For the data with the PPAC this effect is obscured by the larger straggling contribution but again the measured value for C₄H₁₀ at 150 Torr is the only one which is larger than the calculated value. For the data with the PPAC placed in front of the IC, the values of the calculated and measured resolutions increase roughly by a factor of 1.6. This indicates that the PPAC foils will be the limiting factor for the energy resolution at low energies. Therefore, to improve the energy resolution the PPAC foils should be as thin as possible.

4.2. The energy-loss signals

For the data taken at pressures of 38 and 40 Torr, an energy-loss signal can be obtained from the first anode ($\Delta E = E_1 = E_{1L} + E_{1R}$), the sum of the first and second anode ($\Delta E = E_1 + E_2$) and the sum of the first three anodes ($\Delta E = E_1 + E_2 + E_3$). For the data taken at 150 and 160 Torr, the particles were almost stopped under the second anode, so an energy-loss signal can only be obtained from the first anode. The calibration from channels to energy has been discussed in the previous subsection. The measured energy losses (ΔE) are given in table 2 together with calculated energy losses obtained with stopping powers taken from ref. [12]. Table 2 shows that for small energy losses (38 and 40 Torr, E_1) the calculated values agree with the measured values, but that all other calculated values differ by 10% to 30% with the experimental data. Calculations with stopping powers for ¹²C in (CH₂)_n, taken from ref. [19] yielded the same results.

Table 2

The energy loss as a function of the counting gas, the gas pressure (P) and the length of the ΔE anode (L). ΔE : measured energy loss, ΔE_c : calculated energy loss, $\delta \Delta E$: measured energy-loss resolution (fwhm), $\delta \Delta E_n$: noise contribution, $\delta \Delta E_{\text{str}}$: calculated straggling contribution, $\delta \Delta E_{\text{tot}}$: total calculated energy-loss resolution.

Gas	P (Torr)	L (cm)	ΔE (MeV)	ΔE_c (MeV)	$\delta \Delta E$ (keV)	$\delta \Delta E_n$ (keV)	$\delta \Delta E_{\text{str}}$ (keV)	$\delta \Delta E_{\text{tot}}$ (keV)
C ₄ H ₁₀	38	5	2.74	2.65	170	90	180	200
CF ₄	40	5	2.97	2.89	210	120	200	230
C ₄ H ₁₀	38	10	6.66	5.43	250	100	300	320
CF ₄	40	10	7.35	5.93	310	130	320	350
C ₄ H ₁₀	38	30	21.3	18.5	530	110	730	740
CF ₄	40	30	22.8	20.3	590	150	780	790
C ₄ H ₁₀	150	5	16.0	11.7	370	90	530	540
CF ₄	160	5	17.2	12.6	420	120	560	570

The fwhm of the energy-loss distributions ($\delta\Delta E$) are also given in table 2. The major contributions to the energy-loss distribution are: (1) energy straggling under the anodes, (2) the energy spread of the incoming particles and (3) electronic noise. The straggling contribution ($\delta\Delta E_{\text{str}}$) has been calculated accordingly to eqs. (4)–(6) given in the previous subsection. Since there exists a discrepancy between the calculated and measured value of the energy loss the measured value of ΔE has been substituted in eq. (5). The contribution due to the energy spread of the incoming particles should be neglected in comparison to $\delta\Delta E_{\text{str}}$. The contribution due to electronic noise ($\delta\Delta E_n$) has been derived from pulser data. Values for ($\delta\Delta E_{\text{str}}$) and ($\delta\Delta E_n$) are given in table 2 together with their quadratic sum: $\delta\Delta E_{\text{tot}}$. As can be seen in table 2, the values of $\delta\Delta E_{\text{tot}}$ overestimate the data by 20–50%. This must be due to the charge-fluctuation contribution, since in most cases the Bohr straggling could be neglected.

4.3. The position readout

The mask in front of the detector allowed for a measurement of the linearity and resolution of the posi-

tion readout of the IC. Fig. 5 shows a matrix of the measured vertical position (y) versus the measured horizontal position (x). The matrix was accumulated with data from a run with C_4H_{10} at 150 Torr and no PPAC in front of the IC. The 40 holes of the upper part of the mask are clearly visible. Projections of the events onto the x and y axes are also given in fig. 5.

For both gasses and both pressures four x spectra have been accumulated with software gates on the y coordinate, corresponding to each row of holes. Only the runs without PPAC have been considered. The data show that the x linearity and resolution do not depend on the y position.

The calibration factor from channels to mm is obtained by fitting a straight line to the data. With the calibrations, the differences between the calibration curve and the data points have been calculated. The residues obtained in this way are a measure of the linearity of the readout. The maximum residue for C_4H_{10} at both pressures is 2 mm, which is well below the experimental resolution. For CF_4 the maximum residues are about 4 mm.

The x resolution (δx) is given in table 3 for all test runs without PPAC. Two major contributions to the x

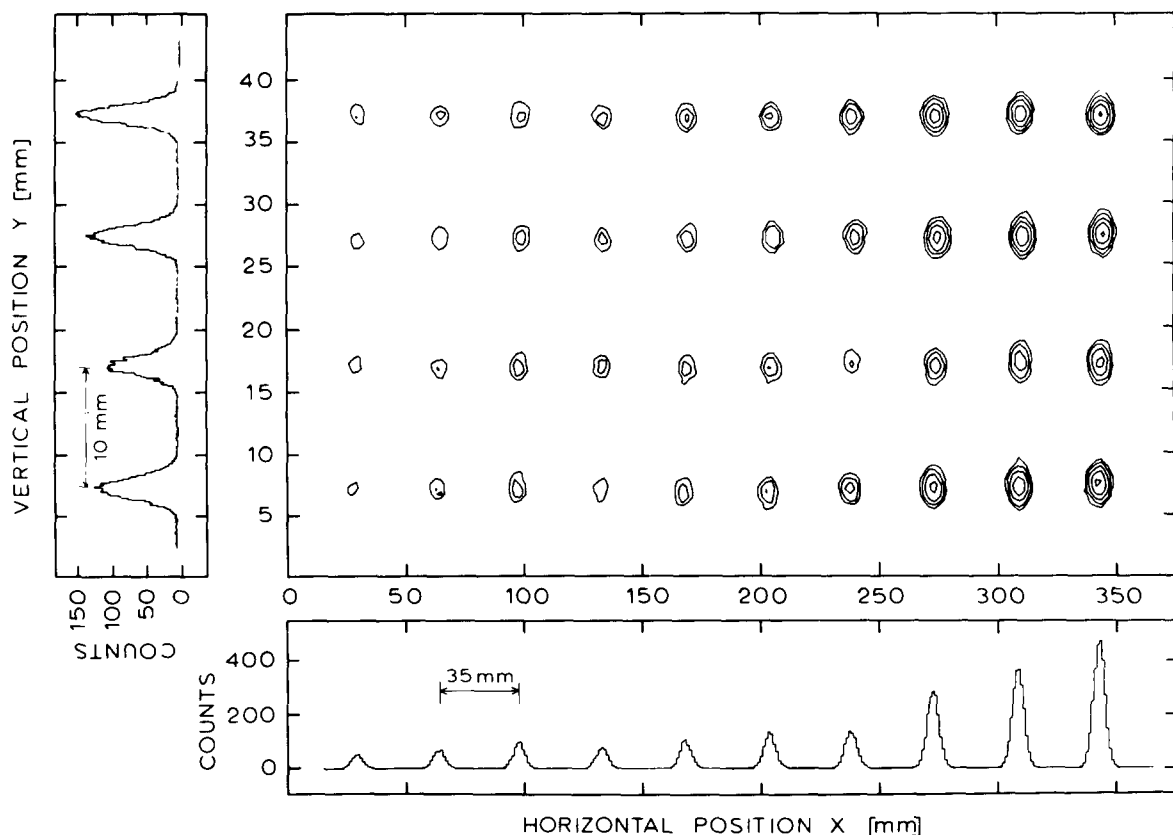


Fig. 5. A matrix of the vertical position (y) against the horizontal position (x). The counting gas was C_4H_{10} at a pressure of 150 Torr. The matrix was accumulated with no constraint on the total energy or on the energy loss. The 40 holes of the upper part of the mask are clearly observed. The spectra are the projections of the matrix on the x and y axes.

Table 3

The results for the horizontal (x) position readout as a function of counting gas and gas pressure (P). δx : measured position resolution, δx_{str} : calculated straggling contribution, δx_n : noise contribution, σ_{min} , σ_{max} : calculated minimum and maximum diffusion width.

Gas	P (Torr)	δx (mm)	δx_{str} (mm)	δx_n (mm)	σ_{min} (mm)	σ_{max} (mm)
C_4H_{10}	38	17	14	17	2.5	10
CF_4	40	17	13	17	2.5	10
C_4H_{10}	150	6.5	6.4	3.4	0.4	1.0
CF_4	160	6.1	6.4	3.9	1.0	1.6

resolution can be given: (1) the energy-straggling contribution δx_{str} , and (2) the noise contribution δx_n .

The straggling contribution can be calculated from eq. (1). The fwhm of the distributions of E_L and E_R (δE_L and δE_R , respectively) are taken to be proportional to the square root of E_R and E_L :

$$\delta E_R = C_e (E_R)^{1/2} \quad \text{and} \quad \delta E_L = C_e (E_L)^{1/2}, \quad (7)$$

where C_e is a factor which has been determined from the data. Then the width in x due to straggling of E_L and E_R (δx_{str}) is given by:

$$\delta x_{\text{str}} = \frac{C_e}{(E_1)^{1/2}} (1 - x^2)^{1/2} \left[1 - \frac{2\sigma}{d(1 - x^2)} \right]. \quad (8)$$

Here, E_1 is the sum of E_L and E_R , d is the width of one segment of the anode (fig. 4) and σ is a measure of the lateral diffusion of the electron cloud as it reaches the anode [10]. Since for CF_4 no values of σ could be found in the literature, the value of δx_{str} has been calculated with $\sigma = 0$ for both gasses, and are given in table 3, transformed to mm.

The noise contribution (δx_n) is given by [10]:

$$\delta x_n = (2)^{1/2} \frac{\delta E_n}{E_1} \left[1 + x_0^2 - \gamma(1 - x_0^2) \right]^{1/2}, \quad (9)$$

where δE_n is the noise of the anode ($\delta E_n = \delta E_{L_n} = \delta E_{R_n}$) and γ is the correlation coefficient between the noise of the left-hand and right-hand side of the anode (δE_{L_n} and δE_{R_n} , respectively). The value of γ has been calculated from pulser data: $\gamma = -0.4$. In eq. (9) a correction factor concerning the capacitances of the left and right side of the anode is omitted since it is close to 1 (for details see ref. [10]). Values of δx_n , calculated from pulser data and transformed to mm are given in table 3.

From table 3 it can be seen that the quadratic sum of the straggling contribution, calculated with $\sigma = 0$, and the noise contribution is larger than the measured resolution (δx). Therefore diffusion of the electron cloud has to be taken into account. From the data and the

calculated values of δx_{str} and δx_n a lower and upper limit for σ could be calculated which are given in table 3. At 150 and 160 Torr the value of σ is a factor 2 larger for CF_4 than for C_4H_{10} . At 38 and 40 Torr the value of σ is of the order of d for both gasses.

Fig. 6 shows the fwhm of the peaks in the spectrum, accumulated with C_4H_{10} at 150 Torr, as a function of the position of the corresponding hole. The lines represent calculations of the fwhm, according to eqs. (8) and (9). For σ values of 0.4 mm and 1.0 mm have been substituted. Fig. 6 shows that the dependence of the x resolution on the horizontal coordinate is well reproduced by the calculation.

For each experimental situation 10 y spectra have been accumulated corresponding to the 10 columns of holes. The differential nonlinearity of the y readout has been found to be less than 1 mm. The y resolution does not depend on the horizontal position and only slightly on the vertical position (10% change over 4 cm). For C_4H_{10} and CF_4 the mean values of the y resolution are: $\delta y = 1.7$ mm and $\delta y = 2.1$ mm, respectively.

The two major contributions to the y resolution are: (1) a source width of approximately 1 mm and (2) the electronic noise. Since no PPAC was used as trigger counter during the test runs, the y position was measured from the time difference between the signal of the cathode preamplifier and the signal of the preamplifier connected to anode A_2 . Because the noise and risetime of the cathode signals were much larger than those of the anode signal, only the noise of the cathode signal contributes. The resulting noise contribution is 1.4 mm for C_4H_{10} and 1.75 mm for CF_4 . Together with the 1 mm source width this roughly explains the experimental data.

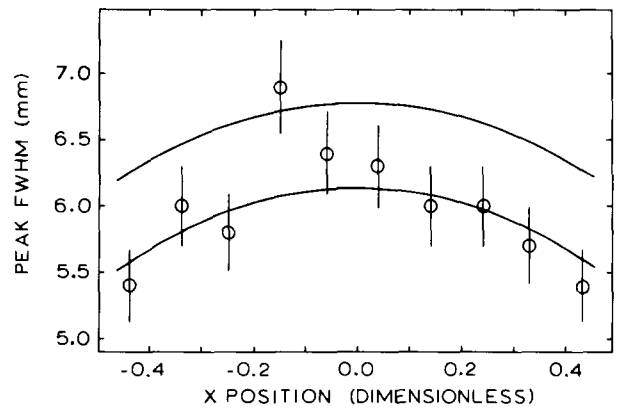


Fig. 6. The fwhm of the peaks in the x -spectrum as a function of the x -position. The counting gas was C_4H_{10} at at pressure of 150 Torr. The two lines give the calculated fwhm according to eqs. (8) and (9), with $\sigma = 0.4$ mm and $\sigma = 1.0$ mm for the upper and lower line, respectively.

Table 4

The time resolution for the small and large PPAC (PPAC₁ and PPAC₂, respectively) measured against a Si detector and against each other, with isobutane as detector gas. E : particle energy, P : gas pressure, V_c : cathode bias, V_{pulse} : estimated pulse height after preamplification (errors are 30%), ΔE : energy loss between the electrode foils and δt : total time resolution.

Particle	E (MeV)	P (Torr)	V_c (V)	V_{pulse} (mV)	ΔE (keV)	δt (ps)	Detectors
^{12}C	38	10	640	150	29	200	PPAC ₁ -Si
		15	760	350	40	200	PPAC ₁ -Si
^{12}C	38	10	630	350	29	400	PPAC ₂ -Si
^4He	5.0	15	720	100	10	800	PPAC ₁ -PPAC ₂
^{12}C	38	12	660	150	33	400	PPAC ₁ -PPAC ₂
^{28}Si	55	10	620	400	130	280	PPAC ₁ -PPAC ₂

5. The performance of the time-of-flight system

The time-of-flight (TOF) system has been tested separately and in conjunction with the IC. In the tests performed without the IC the influence of gas pressure and energy loss on the time resolution has been measured. In a test run with the IC the influence of the position of the particle on the time readout has been studied.

5.1. The time resolution

To measure the time resolution of the small and large PPAC, use has been made of the Enge split-pole spectrograph of the R.J. Van de Graaff Laboratory. The PPACs were placed behind each other in the detector chamber of the spectrograph. The angle with the focal plane was adjusted in such a way that the particles entered the PPAC perpendicular to the foils. The PPAC signals were amplified by a fast current amplifier [20] followed by a timing filter amplifier (TFA, $\tau_{\text{int}} = 2$ ns, $\tau_{\text{dif}} = 50$ ns) and a constant fraction discriminator (CFD, $\tau_{\text{delay}} = 2$ ns). Behind the PPACs a small silicon surface barrier detector (100 μm thick, active area 50 mm^2) was placed.

First the small and large PPAC (PPAC₁ and PPAC₂, respectively) were tested against the Si detector with ^{12}C particles ($E = 39$ MeV). At a pressure of 10 and 15 Torr C_4H_{10} the total time resolution of PPAC₁ and the Si detector was 200 ps. The time resolution of the Si detector for ^{12}C ($E = 34$ MeV) is estimated to be 100 ps, which gives a time resolution of 150 ps for PPAC₁. The time resolution of the large PPAC, measured with ^{12}C particles against the Si detector, is 400 ps. The difference between the resolution of PPAC₁ and PPAC₂ can be explained by the larger capacitance of PPAC₂ (200 pF), which resulted in a larger risetime of 5–10 ns (see section 3). Also, the pulse height was a factor 2 smaller in comparison to PPAC₁.

Secondly the combined time resolution δt of PPAC₁ and PPAC₂ was measured. The Si detector was only used to eliminate the position dependence of the time resolution (see subsection 5.2). The time resolution was measured with α -particles ($E = 5.5$ MeV), ^{12}C ($E = 39$ MeV) and ^{28}Si ($E = 55$ MeV). The results are plotted against $1/\Delta E$ in fig. 7 (ΔE is the energy loss in keV between the PPAC foils). If the pulse height is a linear function of the energy loss between the foils, the relation between $1/\Delta E$ and δt should approximately be a straight line [eq. (3)]. Fig. 7 shows that the data points are consistent with a straight line. An estimate of the time resolution can be given by:

$$\delta t(\text{ps}) = 240 + \frac{5600}{\Delta E(\text{keV})}. \quad (10)$$

The best time resolution that can be obtained with the TOF system is therefore $250 (\pm 50)$ ps.

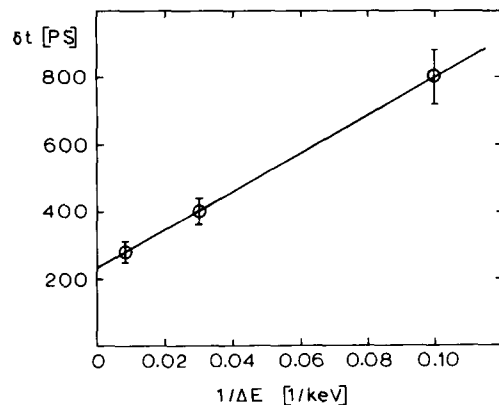


Fig. 7. The time resolution of the TOF system as a function of the energy loss ΔE between the electrode foils of a PPAC. The line is a linear fit to the data.

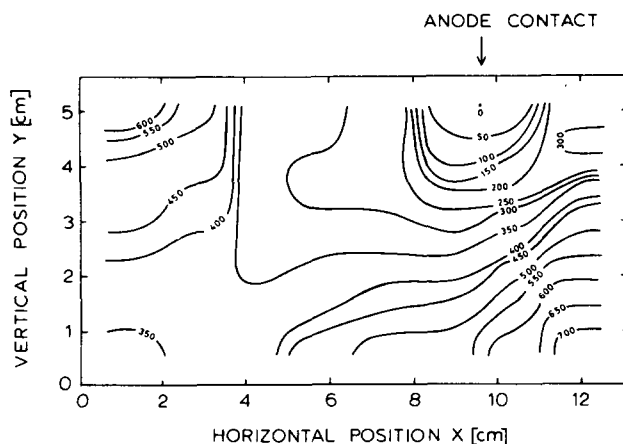


Fig. 8. The position dependence of the time difference Δt between PPAC₁ and PPAC₂. The time difference corresponding to $x = 9.6$ cm and $y = 5.1$ cm has been subtracted to show more clearly the time walk. The numbers give the time walk in ps for the corresponding lines.

5.2. The position dependence of the time signal

To measure the position dependence of the time signals of the TOF system the complete setup of IC and TOF system was used. In this test run the large PPAC was electrically divided in three parts with an active area of 12 by 12 cm² each. The PPACs were filled with C₄H₁₀ at a pressure of 10 Torr. The mask in front of the IC was removed. The IC was filled with C₄H₁₀ at a pressure of 110 Torr. The settings of the TFAs and CFDs of the TOF system were as described in section 5.1. Carbon particles ($E = 39$ MeV) were elastically scattered from a gold target. The time difference between the two PPACs (Δt) and the data from the IC were written on tape in event by event mode. In this way it is possible to obtain the time difference Δt between the start and stop PPAC as a function of the x and y position, measured by the IC. Fig. 8 shows a contour map of Δt as a function of x and y . The time difference corresponding to $x = 9.6$ cm and $y = 5.1$ cm was subtracted to show more clearly the spread in Δt . Concentric rings around the anode contact screw are clearly observed. The walk in Δt has a maximum of 700 ps for this area. Therefore, in order to obtain a time resolution of less than 500 ps, it will be necessary to calibrate the TOF system with particles which have a well defined velocity (e.g. beam particles elastically scattered from Au).

6. Concluding remarks

The test experiments with ¹²C ($E = 39$ MeV) ions have shown that the energy and position resolution of

the IC can be calculated within an accuracy of 10–20%. There is a discrepancy between the measured and calculated energy-loss signal (10–30%) as well as between the measured and calculated energy-loss resolution (20–50%). The energy resolution calculated for particles with a mass between 20 and 40 and an energy between 5 and 30 MeV varies between 0.1 and 2%. It is mainly determined by the energy straggling in the PPAC foils. Since the energy signals depend slightly on the horizontal and vertical position, this energy resolution can only be obtained after a calibration of the active area of the IC. Calculations show that separation of nuclear charge will be possible up to $Z = 20$. The position resolution will be better than 0.5° in almost all cases.

The time resolution of the tof system has been shown to depend on the energy loss between the PPAC foils; it varies between 280 ps (²⁸Si at 55 MeV) and 800 ps (α at 5 MeV). These results can only be obtained after a position-dependent correction for the time delay in the large PPAC. Combining the calculated energy resolution with the time resolution it has been calculated that with the 1.7 m flight path mass separation will be possible up to the projectile mass even at the highest energies.

The large solid angle of the system, the absence of radiation damage and the good energy, position, nuclear charge and mass resolution make the detection system especially useful for correlation studies.

We gratefully acknowledge the cooperation of G. Augustinski, H. Daues, H. Sann and H. Stelzer of GSI, Darmstadt in supplying the drawings of the “Mammut” detector and supporting us with advice concerning details of the design of the IC and the PPACs. We also would like to thank H. v.d. Blij (KVI, Groningen) for constructing the PPACs and the workshop of NIKHEF-H (Amsterdam) for manufacturing the Frisch grids. This work was performed as part of the research program of the “Stichting voor Fundamenteel Onderzoek der Materie” (FOM) with financial support from the “Nederlandse Organisatie voor Zuiver-Wetenschappelijk Onderzoek” (ZWO).

References

- [1] M.J. Murphy, B.G. Harvey, D.L. Hendrie, W.W. Pang, K. van Bibber and R. Legrain, Phys. Lett. 120B (1983) 75.
- [2] P.L. Gonthier, H. Ho, M.N. Namboodiri, J.B. Natowitz, L. Adler, S. Simon, K. Hagel, S. Kniffen and A. Khodai, Nucl. Phys. A411 (1983) 289.
- [3] B. Martin and H. Stelzer, in Experimental methods in heavy ion physics, ed., K. Bethge, Lecture Notes in Physics 83 (Springer, 1978).
- [4] H. Sann, H. Damjantschitz, D. Hebbard, J. Junge, D. Pelte, B. Povh, D. Schwalm and D.B. Tran Thoi, Nucl. Instr. and Meth. 124 (1975) 509.

- [5] G. Augustinski, Mammut, Internal Report GSI, Darmstadt (1981).
- [6] H. Stelzer, Preprint GSI-82-39, GSI, Darmstadt (1982).
- [7] K. Kusterer, J. Betz, H.L. Harney, B. Heck, Liu Ken Pao and F. Porto, Nucl. Instr. and Meth. 177 (1980) 485.
- [8] H.W. Fullbright, Nucl. Instr. and Meth. 162 (1979) 21.
- [9] H. Stelzer, Nucl. Instr. and Meth. 133 (1976) 163.
- [10] G. Rosner, B. Heck, J. Pochodzalla, G. Hlawatsch, B. Kolb and A. Miczaika, Nucl. Instr. and Meth. 188 (1981) 561.
- [11] MKS Instruments Inc., Burlington, USA.
- [12] H.H. Andersen and J.F. Ziegler, The stopping and ranges of ions in matter, vol. 3, ed., J.F. Ziegler (Pergamon, New York, 1977).
- [13] A. Breskin, Nucl. Instr. and Meth. 196 (1982) 11.
- [14] V. Palladino and B. Sadoulet, Nucl. Instr. and Meth. 128 (1975) 323.
- [15] R.J. Elsenaar: the SPECTR system, Annual report of the R.J. Van de Graaff Laboratory, Utrecht (1982) p. 64.
- [16] F. Sauli, CERN Report 77-09 (1977).
- [17] H. Schmidt-Böcking, in Experimental methods in heavy ion physics, ed., K. Bethge, Lecture Notes in Physics 83 (Springer, 1978).
- [18] H. Schmidt-Böcking and H. Hornung, Z. Physik A286 (1978) 253.
- [19] L.C. Northcliffe and R.F. Schilling, Nucl. Data Tables A7 (1970) 233.
- [20] Elektronik Service Nöggerath, Darmstadt, Germany.